An effective fluid model for the bending failure of level ice

Keijdener, Chris; Hendrikse, Hayo; Metrikine, Andrei

Publication date
2019

Document Version
Final published version

Published in
POAC 2019 - 25th International Conference on Port and Ocean Engineering under Arctic Conditions

Citation (APA)
Keijdener, C., Hendrikse, H., & Metrikine, A. (2019). An effective fluid model for the bending failure of level ice. In *POAC 2019 - 25th International Conference on Port and Ocean Engineering under Arctic Conditions: June 9-13, 2019, Delft, The Netherlands* (Vol. 2019-June)

Proceedings of the 25th International Conference on
Port and Ocean Engineering under Arctic Conditions
June 9-13, 2019, Delft, The Netherlands

An effective fluid model for the bending failure of level ice

Chris Keijdener[1], Hayo Hendrikse[1], Andrei Metrikine[1]
[1] Delft University of Technology, Delft, The Netherlands

ABSTRACT

In this paper, the efficacy of an effective fluid model (EFM) is studied for replicating the effects that hydrodynamics has on the interaction between level ice, modeled as a semi-infinite Kirchhoff-Love plate, and a downward sloping structure, modeled as a rigid and immobile body. The proposed EFM is based on a distributed frequency-independent added mass and damping coefficient, as well as a damper located at the point of contact with the structure. The optimal value of the three coefficients of the EFM is obtained by minimizing the error of the predicted breaking length and maximum contact force over a range of ice velocities when compared to a true hydrodynamics ISI model that is based on incompressible potential flow. The resulting effective hydrodynamic ISI model has greatly improved performance compared to an ISI model that only accounts for hydrostatics, even when the parameters of the system are changed. Moreover, it is much easier to implement and has significantly faster calculation times than the true hydrodynamic ISI model.

KEY WORDS: Effective fluid modeling; hydrodynamics; bending failure; ice-slope interaction.

INTRODUCTION

Due to the increase in global temperatures and the resulting reduction in sea ice cover, the Arctic region is becoming more accessible for shipping, tourism and hydrocarbon extraction. All three opportunities rely heavily on floating structures and these structures are generally equipped with a downward sloping hull in order to minimize the ice loads. This makes it paramount to both understand and be able to predict ice-slope interaction.

Due to the limited availability of full-scale data and the expenses associated with obtaining model scale data, numerical models are still the most common method to study ice-slope interaction. Hydrodynamics has been shown to be a key component of such a model (Valanto 1992; Valanto 2001; Valanto 2006). Through both numerical and experimental modeling, Valanto identified that the inertia of the water plays an important role, even at low interaction velocities. These findings are confirmed by more recent studies (Sawamura et al. 2008; Wang & Poh 2017; Keijdener et al. 2018).

Despite this evidence showing its importance, the majority of ice-slope interaction models do not account for hydrodynamics. In a recent study by (Keijdener et al. 2018), it is shown that excluding hydrodynamics results in an underprediction of the contact load which, in turn, causes an overprediction of the breaking length, with errors up to 100% depending on the ice velocity being considered. It is, therefore, paramount to improve the adoption rate of

hydrodynamics in ice-floater interaction models. In the author's opinion, one of the main reasons for the prevalence of hydrostatic models is the practical issue associated with implementing hydrodynamics. One approach to overcome this issues is to use effective fluid models (EFM). These models aim to capture the effects that hydrodynamics has on ice-slope interaction in an effective manner. However, in contrast to true hydrodynamic models, their effective nature means that they remain very simple, making it trivial to implement them.

A common type of EFM that has been used previously is a frequency-independent added mass coefficient. This EFM can be added to a beam or plate model, thereby obtaining a complete ice-slope interaction model. One of the first to use such a frequency-independent added mass coefficient was (Sørensen 1978). The value of this coefficient was set to the value of a rotating plate obtained by (Engelund 1966). Such an EFM was also used to model the dynamical uplift of level ice (Zhao & Dempsey 1992; Dempsey & Zhao 1993; Zhao & Dempsey 1996). In this series of papers, it was concluded that the fluid underneath the ice significantly increases the amount of mass and damping experienced by the ice. Various values of the added mass coefficient were investigated and the predictions of the resulting model were compared to the predictions of a model that includes hydrodynamic based on incompressible potential flow. It was concluded that a constant added mass coefficient cannot capture the time- and spatial dependence of the mass and damping introduced by hydrodynamics. In a study by (Lubbad et al. 2008), the efficacy of an EFM based on a constant added mass coefficient in combination with a damping term that has a second order dependence on the velocity was investigated. This study concluded that the accuracy of the effective model is lacking compared to a reference model that includes hydrodynamics.

In this paper, an attempt is made to create an EFM that is based on a frequency-independent added mass and damping coefficients. This EFM is added to a 2D Kirchhoff-Love plate that is supported by a Winkler foundation, resulting in a complete 2D ice-slope interaction model. The optimal value of the coefficients of this EFM is found by minimizing the discrepancy between the predictions of this model with respect to the predictions of a reference ice-slope interaction model that includes hydrodynamic based on incompressible potential flow.

The hydrodynamic reference model is introduced first. Thereafter, the proposed EFM is discussed and the scheme that was used to determine the optimal values of its coefficients is explained. The efficacy of the resulting effective ice-slope interaction model is then studied for a wide range of parameters. Lastly, the results are discussed and the conclusions are given.

THE HYDRODYNAMIC REFERENCE MODEL

The 2D hydrodynamic reference model is introduced first. In this paper, only the model description is covered. The solution method based on the pseudo-force approach is not covered and the reader is referred to (Keijdener et al. 2018) for the details.

An overview of the reference model is given in Fig. 1. In this model, the ice is present for $x \leq 0$ and is modeled as a semi-infinite Kirchhoff-Love plate. As no ice is present for $x > 0$, the fluid has a free surface in that region. The ice moves towards the structure with a constant velocity V_{ice}. It is assumed that the interaction between the fluid and the structure can be ignored. Therefore, the structure's geometry is not included in the mathematical model of the fluid. For the interaction with the ice, the structure is modeled as an immovable and rigid body with its geometry reduced to an inclined line that has an angle θ with respect to the x-axis and that passes through the point $x = z = 0$. Due to its forward velocity, the ice impacts the hull. This resulting interaction is resolved using a contact model that penalizes overlap between the ice and the structure. The ice continues to slide down the hull until it fails in bending.

An overview of the mathematical model is given next, starting with the equations governing the fluid and followed by those of the ice.

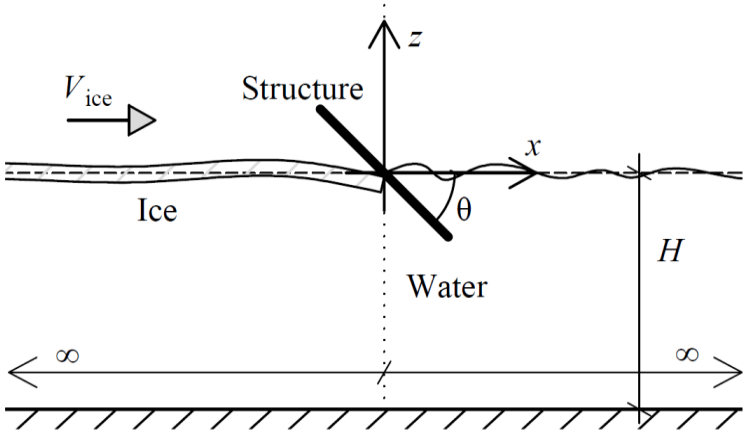

Figure 1. The incoming ice floe moves towards the structure with a constant velocity V_{ice} . For the interaction with the ice, the structure is idealized as an immovable and rigid body with its geometry idealized to an inclined line. The ice slides downwards along this line until it fails in bending.

Governing equations of the fluid

The fluid is modeled as an incompressible potential flow and is, therefore, governed by the Laplace equation. The fluid layer is of finite depth H and the rigid boundary at the bottom prevents penetration of the fluid into the seabed. The fluid pressure $p(x,z,t)$ is modeled using the linearized Bernoulli equation for unsteady potential flow (Stoker 1992), given that the nonlinear term was shown to be of negligible importance for ice-slope interaction (Keijdener et al. 2018). This results in the following three equations:

$$\Delta\dot{\phi}(x,z,t)=0 \quad \forall\, x\in(-\infty,\infty)\cap z\in(-H,0) \tag{1.1}$$

$$\frac{\partial\phi(x,-H,t)}{\partial z}=0 \quad \forall\, x\in\left(-\infty,\infty\right) \tag{1.2}$$

$$p(x,z,t)=-\rho_{w}\left(\ddot{\phi}+g\frac{\partial\phi}{\partial z}\right) \tag{1.3}$$

where $\phi(x,z,t)$ is the displacement potential of the fluid (Jensen et al. 2011), ρ_{w} is the fluid's density, g the gravitational constant, the dot denotes derivatives with respect to time, and round brackets denote an open interval while square brackets, in the equations to follow, denote a closed interval. Note that the first term on the right-hand side of Eq. (1.3), $-\rho_{w}\ddot{\phi}$, is responsible for hydrodynamic effects while the second term, $-\rho_{w}g\frac{\partial\phi}{\partial z}$, is responsible for the hydrostatic effects. By disabling the first term, a hydrostatic model can be obtained.

Governing equations of the ice

The ice interacts with the fluid along their interface located at $x\le 0\cap z=0$. Consequently, the equation of motion of the ice includes the pressure exerted by the fluid. Outside this region, no ice is present and the fluid satisfies the pressure release condition. As the draft of the ice can be ignored, as was shown by (Williams & Squire 2008), the boundary condition of the ice can be formulated at $z=0$:

$$p(x,0,t) = \begin{cases} \rho_i h\ddot{w} + \rho_i \dfrac{h^3}{12}\ddot{w}'' + D_i w'''' & \forall\ x \in (-\infty, 0) \\ 0 & \forall\ x \in (0, \infty) \end{cases} \tag{1.4}$$

where the prime denotes a spatial derivative, ρ_i is the density of the ice, h its thickness, $w(x,t)$ its vertical displacement, $D_i = Eh^3/12/(1-\nu^2)$ its bending stiffness, with E being the ice's Young's modulus and ν its Poisson ratio. Note that D_i aims to capture the bending behavior of level ice, including any variation of temperature, stiffness or any other property across its thickness, in an effective manner, similar to what is done for functionally graded materials. The rotational inertia of the ice and the effect of the axial compression on the vertical motions of the ice are ignored as both terms were shown to be of negligible importance (Keijdener et al. 2018). Next, as cavitation is not accounted for, continuity between ice and fluid dictates that their vertical displacements must be the same along their interface:

$$w(x,t) = \frac{\partial \phi(x,0,t)}{\partial z} \qquad \forall\ x \in (\infty, 0] \tag{1.5}$$

Lastly, two boundary conditions are needed at $x = 0$ to complete the description of the ice. The ice interacts with the structure at this boundary. The contact pressure resulting from this interaction is integrated and translated to the neutral axis of the plate, resulting in vertical force $F_{ct,z}$ and moment M_{ct}. These interaction loads are accounted for in the boundary conditions of the plate which assure a balance of forces and moments at the plate's edge:

$$\begin{aligned} D_i \frac{\partial^3 w(0,t)}{\partial x^3} &= \left(F_{ct,z}(t, w, w', \dot{w}, \dot{w}')\right)\Big|_{x=0} \\ D_i \frac{\partial^2 w(0,t)}{\partial x^2} &= \left(M_{ct}(t, w, w', \dot{w}, \dot{w}')\right)\Big|_{x=0} \end{aligned} \tag{1.6}$$

The contact model used to calculated these loads is described in (Keijdener & Metrikine 2014). This contact model is piece-wise linear in time as it switches between two linear modes of interaction. As the moment of transition between the two modes is not known in advance, the contact model is nonlinear in time. At $x = -\infty$ the plate satisfies the Sommerfeld radiation condition, assuring that the displacements are finite and that no energy is radiated from $x = -\infty$.

The ice slides down the structure until it fails in bending. Failure is defined as the moment in time t_{fail} when the axial stresses due to bending first exceed the ice's flexural strength σ_{fl}:

$$\sigma_{max}(x,t) = \left|\frac{Eh}{2(1-\nu^2)} w''(x,t)\right| \leq \sigma_{fl} \tag{1.7}$$

where the max-subscript implies the maximum axial stress within the cross-section of the ice.

The hydrodynamic reference model introduced in this section is referred to as $\mathcal{M}_{HD}$ in the remainder of this paper. The same model but with hydrodynamics disabled, i.e. with the first term on the right-hand side of Eq. (1.3) disabled, will be referred to as the hydrostatic model $\mathcal{M}_{HS}$.

DESCRIPTION OF THE EFFECTIVE FLUID MODEL

It has been shown that the effect of hydrodynamics on ISI is of the added mass and added damping type (Valanto 1992; Dempsey & Zhao 1993; Keijdener et al. 2018). For this reason, the EFM proposed in this study is based on a frequency-independent added mass and a frequency-independent added damping coefficient. By constructing the EFM in this manner, it is trivial to add it to an existing ice-slope interaction model that only accounts for hydrostatics. In this paper, the EFM is added to $\mathcal{M}_{\mathrm{HS}}$. By augmenting $\mathcal{M}_{\mathrm{HS}}$ with this EFM, an ice-slope interaction model is obtained that includes all four essential components as identified in (Keijdener et al. 2018), namely bending, hydrodynamics, the inertia of the ice, and hydrostatics. The resulting effective ice-slope interaction model will be referred to as $\mathcal{M}_{\mathrm{eHD}}$.

By disabling the hydrodynamic term in Eq. (1.4), $-\rho_{\mathrm{w}}\ddot{\phi}$, substituting the interface condition in Eq. (1.5), and adding the frequency-independent added mass and added damping coefficient, the equation of motion of $\mathcal{M}_{\mathrm{eHD}}$ is obtained:

$$\rho_{\mathrm{i}} h(1+C_m)\ddot{w} + 2\xi_{\mathrm{d}} C_{\mathrm{crit}}\dot{w} + D_{\mathrm{i}} w'''' + \rho_{\mathrm{w}} g w = 0 \tag{1.8}$$

where $C_{\mathrm{crit}} = \sqrt{\rho_{\mathrm{i}} h \rho_{\mathrm{w}} g}$. C_m and ξ_{d} are the unknown dimensionless added mass and added damping coefficients, where the latter is expressed in terms of critical damping, analogous to a damped harmonic oscillator. The value for these coefficients is obtained using the optimization scheme that is explained in the next section.

$\mathcal{M}_{\mathrm{eHD}}$ has two unknown coefficients, namely c_m and ξ_{d}. To further improve the efficacy of the EFM, a dashpot is added at the boundary of the ice that is located at $x = 0$. This dashpot could capture the radiation of energy into the open-water region through surface waves. However, the importance of wave radiation on the ice-slope interaction is unclear as in (Keijdener et al. 2018) it is concluded that radiation damping does not have a significant impact on the interaction while (Sawamura et al. 2008) found a 40% reduction in the displacements of the ice when disabling wave radiation. Despite lacking a clear physical substantiation for this dashpot, its addition does not significantly affect the computational efficiency of the EFM and is, therefore, an efficient way to improve its efficacy. Eqs. (1.6) are updated accordingly:

$$\begin{aligned} D_{\mathrm{i}} \frac{\partial^3 w(0,t)}{\partial x^3} + C_{\mathrm{bc}} C_{\mathrm{crit}} \dot{w}(0,t) &= \left(F_{\mathrm{ct,z}}(t, w, w', \dot{w}, \dot{w}') \right)\Big|_{x=0} \\ D_{\mathrm{i}} \frac{\partial^2 w(0,t)}{\partial x^2} &= \left(M_{\mathrm{ct}}(t, w, w', \dot{w}, \dot{w}') \right)\Big|_{x=0} \end{aligned} \tag{1.9}$$

where C_{bc} is the unknown damping coefficient of the dashpot with dimensions m^2. As the addition of the dashpot may not be desirable from a physical point of view, the optimization of the EFM's coefficients will be done twice, once with $C_{\mathrm{bc}} = 0$ and once with $C_{\mathrm{bc}} \neq 0$.

OPTIMIZATION

The optimal value of the coefficients of the EFM, C_m, ξ_d and C_bc, are found through an optimization process. The goal of this process is to find the set of coefficients that results in the smallest discrepancy between the predictions of $\mathcal{M}_\mathrm{eHD}$ and the predictions of the reference hydrodynamic model $\mathcal{M}_\mathrm{HD}$ that was introduced previously. The predictions that will be considered are the breaking length as a function of ice velocity $l_\mathrm{br}(V_\mathrm{ice})$ and the maximum contact force that occurred during the interaction as a function of ice velocity $F_\mathrm{max}(V_\mathrm{ice})$ as these are important aspects of ice-slope interaction. Based on these two predictions, the discrepancy is quantified using the dimensionless error ε that is defined as:

$$\varepsilon = \mathrm{rms}\left(\frac{l_\mathrm{br}(V_\mathrm{ice}) - l_\mathrm{br}^{\mathrm{HD}}(V_\mathrm{ice})}{l_\mathrm{br}^{\mathrm{HD}}(V_\mathrm{ice})}\right) + \mathrm{rms}\left(\frac{F_\mathrm{max}(V_\mathrm{ice}) - F_\mathrm{max}^{\mathrm{HD}}(V_\mathrm{ice})}{F_\mathrm{max}^{\mathrm{HD}}(V_\mathrm{ice})}\right) \tag{1.10}$$

where the four terms with the HD superscript are the predictions of $\mathcal{M}_\mathrm{HD}$ and the remaining two terms are the predictions of $\mathcal{M}_\mathrm{eHD}$.

The following bounds are used for the parametric space wherein the optimal values are being sought: $0 \le C_m \le 12$, $0 \le \xi_\mathrm{d} \le 4.5$ and $0 \le C_\mathrm{bc} \le 12 \cdot 10^{-6}$ m^2. These bounds were chosen to assure that the optimal set of coefficients falls within the search space. The volume is discretized using a step size of 2, 0.5 and $2 \cdot 10^{-6}$ m^2 respectively, resulting in 420 grid points. Spline interpolation is then used to interpolate between the grid points to find the set of two (or three) coefficients that leads to the smallest error ε.

RESULTS

The results are presented next. First, the effect of each coefficient on the predictions of $\mathcal{M}_\mathrm{eHD}$ is studied. Thereafter, the optimization is done for the set of default parameters of the system that is listed below. Noting that the optimal value of the coefficients will change depending on the physical parameter of the system used, the sensitivity of the coefficients to changes in the physical parameters is studied.

The following set of default parameters are used (Keijdener et al. 2018): $h = 1$ m, $\rho_\mathrm{i} = 925$ kg/m^3, $\rho_\mathrm{w} = 1025$ kg/m^3, $g = 9.81$ m/s^2, $H = 100$ m, $E = 5$ GPa, $\nu = 0.3$, $\sigma_\mathrm{c} = 600$ kPa, $\sigma_\mathrm{fl} = 500$ kPa, ice-steel friction coefficient 0.1, hull angle $\theta = 45^\circ$, $V_\mathrm{ice} = [0, 0.5]$ m/s, the number of fluid modes set to $N_\mathrm{k} = 250$ and an initial time step $\Delta_\mathrm{t} = 10^{-3}$ s. The time step was adaptively shortened to assure convergence for all cases considered in this paper.

The effect of each coefficient on the predictions

The effective fluid model has three coefficients. The effect of each coefficient on the predictions of $\mathcal{M}_\mathrm{eHD}$ is presented next.

The effect of C_m on the predictions of $\mathcal{M}_\mathrm{eHD}$ is shown in Fig. 2. The additional mass increases the magnitude of the peak in the contact force that occurs during the initial impact, as can be seen in the bottom graph. This increase in peak force is also reflected in the middle graph by an increase in $F_\mathrm{max}(V_\mathrm{ice})$ and causes the ice floe to fail dynamically at lower ice velocities, thereby reducing the transition velocity $V_{\mathrm{s}\to\mathrm{d}}$ that marks the transition from static to dynamic failure. This trend can be observed in the top graph which shows that as C_m

increases, $V_{\mathrm{s}\to\mathrm{d}}$ of $\mathcal{M}_{\mathrm{eHD}}$, $V_{\mathrm{s}\to\mathrm{d}}^{\mathrm{eHD}}$, decreases and approaches that of the reference model $V_{\mathrm{s}\to\mathrm{d}}^{\mathrm{HD}}$.

The effect of ξ_{d} on the predictions of $\mathcal{M}_{\mathrm{eHD}}$ is shown on the left-hand side in Fig. 3. First, the bottom graph shows that increasing ξ_{d} smoothens $F_{\mathrm{ct}}(t)$. This, in turn, has a smoothening effect on $F_{\max}(V_{\mathrm{ice}})$ and $l_{\mathrm{br}}(V_{\mathrm{ice}})$ when $V_{\mathrm{ice}} \approx V_{\mathrm{s}\to\mathrm{d}}^{\mathrm{eHD}}$, as is evident from the top and middle graph. Second, the added damping results in a slight increase in $F_{\mathrm{ct}}(t)$, resulting in a slight increase in $F_{\max}(V_{\mathrm{ice}})$ and a shorter $l_{\mathrm{br}}(V_{\mathrm{ice}})$.

The effect of C_{bc} on the predictions of $\mathcal{M}_{\mathrm{eHD}}$ is shown on the right-hand side in Fig. 3. The bottom graph shows that increasing C_{bc} has a smoothing effect on $F_{\mathrm{ct}}(t)$, similar to ξ_{d}. However, as the dashpot is only present at $x=0$ whereas ξ_{d} is present $\forall\, x \le 0$, the dashpot has a strong effect on $F_{\max}(V_{\mathrm{ice}})$ and only a weak effect on $l_{\mathrm{br}}(V_{\mathrm{ice}})$. Its effects on $l_{\mathrm{br}}(V_{\mathrm{ice}})$ are limited as the breakage of the ice is mainly driven by the distributed terms, i.e. c_m and ξ_{d}, as shown previously.

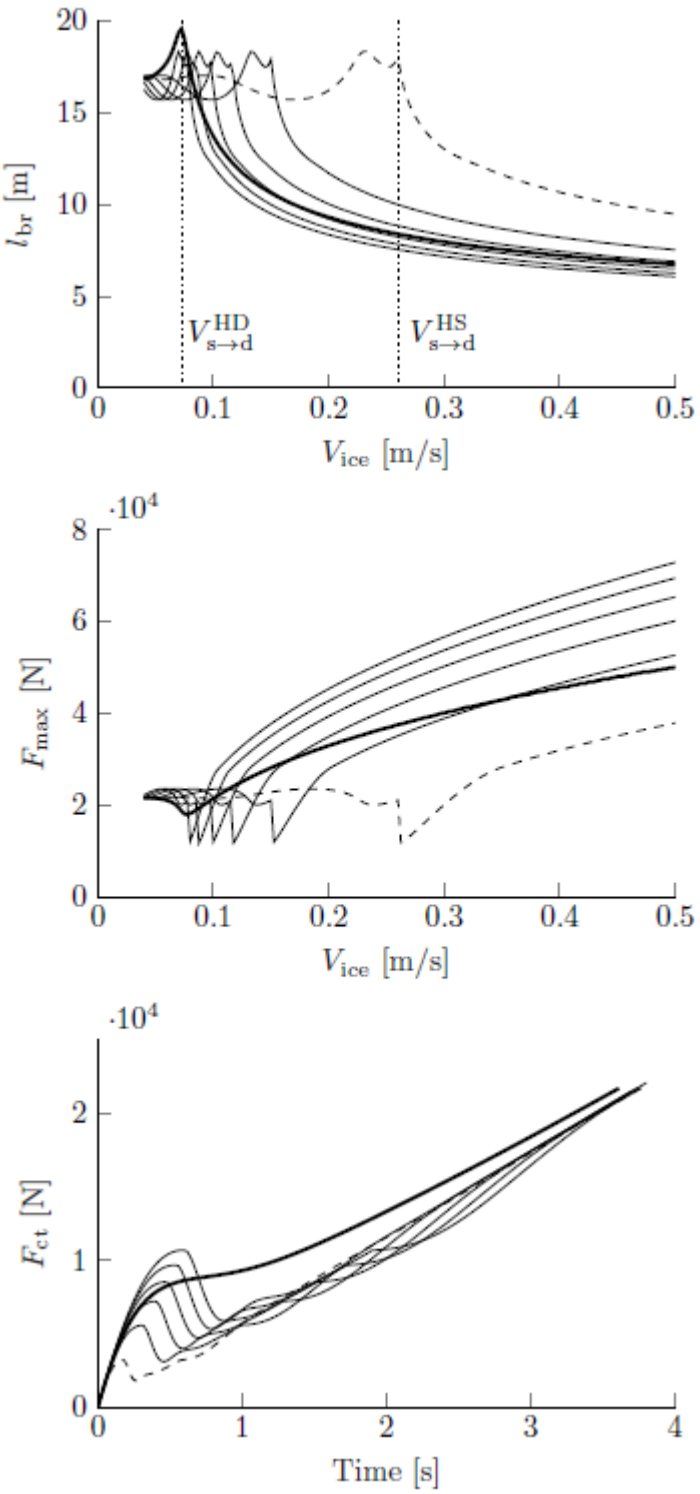

Figure 2. The effect of C_m on the predictions of $\mathcal{M}_{\mathrm{eHD}}$. The bold curves show $\mathcal{M}_{\mathrm{HD}}$. The dashed curve shows $\mathcal{M}_{\mathrm{eHD}}\left(C_m = \xi_{\mathrm{d}} = C_{\mathrm{bc}} = 0\right) = \mathcal{M}_{\mathrm{HS}}$. All subsequent solid curves are evaluations at $C_m = \{2,4,6,8,10\}$ respectively. For the bottom graph $V_{\mathrm{ice}} = 0.04$ m/s.

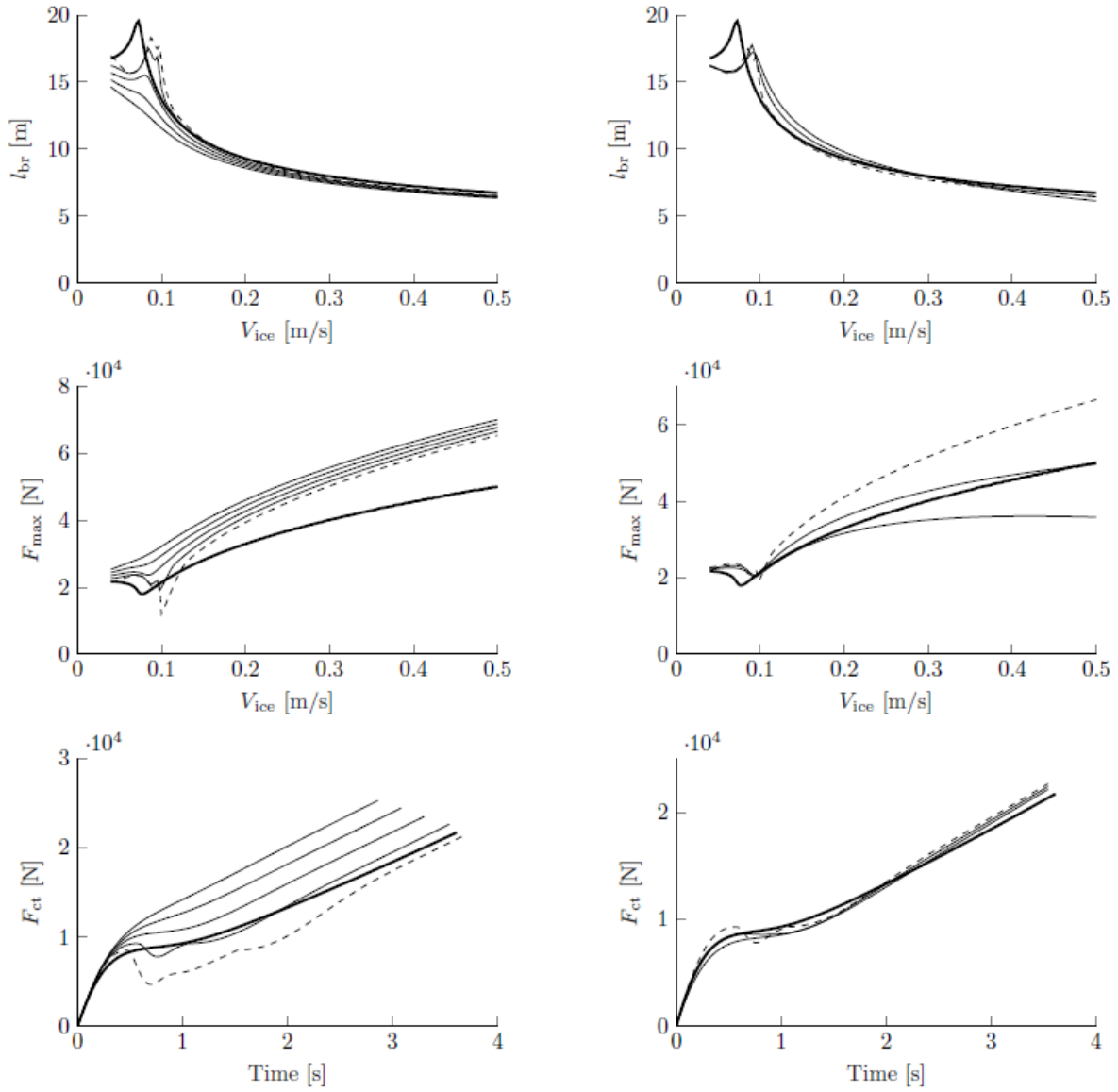

Figure 3. **Left**: The effect of ξ_d on the predictions of $\mathcal{M}_{eHD}$. The bold curves show $\mathcal{M}_{HD}$. The dashed curve shows $\mathcal{M}_{eHD}\left(C_m = 6.26, \xi_d = C_{bc} = 0\right) \neq \mathcal{M}_{HS}$. All subsequent solid curves are evaluations at $\xi_d = \{1,2,3,4\}$ respectively. For the bottom graphs $V_{ice} = 0.04$ m/s. **Right**: The effect of C_{bc} on the predictions of $\mathcal{M}_{eHD}$. The bold curves show $\mathcal{M}_{HD}$. The dashed curve shows $\mathcal{M}_{eHD}\left(C_m = 6.26, \xi_d = 1.06, C_{bc} = 0\right) \neq \mathcal{M}_{HS}$. All subsequent solid curves are evaluations at $C_{bc} = \{4,8\} \cdot 10^{-6}\,\mathrm{m}^2$ respectively. For the bottom graph $V_{ice} = 0.04$ m/s.

Optimal sets of coefficients

Based on the optimization process described above, the optimal sets of coefficients were determined. The optimal set with $C_{bc} = 0$ will be referred to as $\mathcal{P}$ while the optimal one with $C_{bc} \neq 0$ will be referred to as $\mathcal{P}^*$. The optimization was done for the default set of parameters, leading to the following optimal sets: $\mathcal{P}_{def} = \{C_m = 2.83, \xi_d = 1.46, C_{bc} = 0\ \mathrm{m}^2\}$ and $\mathcal{P}^*_{def} = \{C_m = 6.26, \xi_d = 1.06, C_{bc} = 4.85 \cdot 10^{-6}\ \mathrm{m}^2\}$. The performance of $\mathcal{M}_{eHD}\left(\mathcal{P}_{def}\right)$ and $\mathcal{M}_{eHD}\left(\mathcal{P}^*_{def}\right)$ is shown in Fig. 4. The figure shows that the prediction of $\mathcal{M}_{eHD}\left(\mathcal{P}_{def}\right)$ are

significantly better than those of $\mathcal{M}_{\text{HS}}$ and that the predictions of $\mathcal{M}_{\text{eHD}}\left(\mathcal{P}_{\text{def}}^{*}\right)$ are slightly better still.

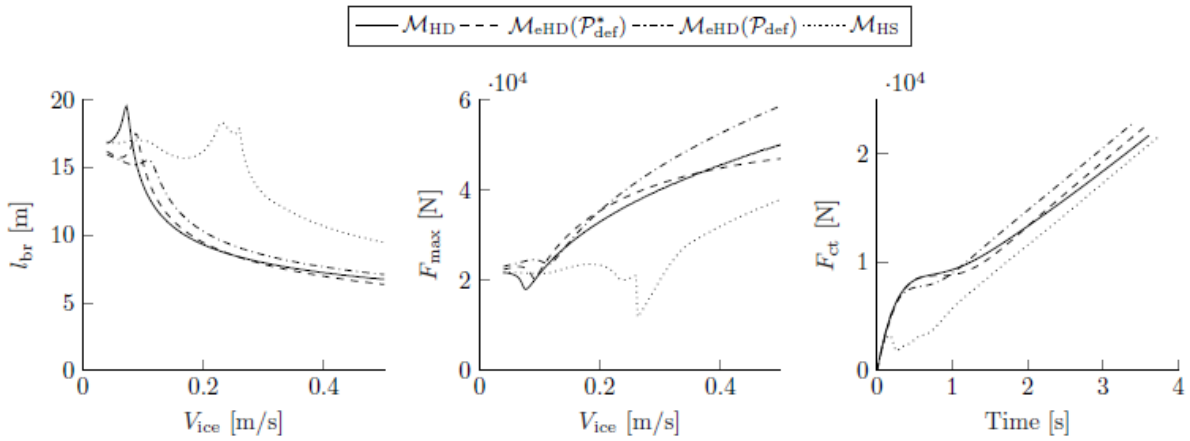

Figure 4. The performance of $\mathcal{M}_{\text{eHD}}\left(\mathcal{P}_{\text{def}}\right)$, $\mathcal{M}_{\text{eHD}}\left(\mathcal{P}_{\text{def}}^{*}\right)$ and $\mathcal{M}_{\text{HS}}$. For the right graph $V_{\text{ice}} = 0.04$ m/s.

Sensitivity analysis

As the predictions of the reference model $\mathcal{M}_{\text{HD}}$ depend on the physical parameters of the system, the optimal set of coefficients will be different for each set of physical parameters used. However, as having parameter-dependent coefficients is impractical, the option of using $\mathcal{M}_{\text{eHD}}\left(\mathcal{P}_{\text{def}}\right)$ and $\mathcal{M}_{\text{eHD}}\left(\mathcal{P}_{\text{def}}^{*}\right)$ independently of changes to the physical parameter is explored. Since these two sets become suboptimal when the physical parameters of the system are changed, the error ε, see Eq. (1.10), of both models will increase. This increase in error is shown in Table 1. All parameters were set to their default values, except for the parameter listed in the left column which was set to the specified value.

Increase in error when using $\mathcal{P}_{\text{def}}$ and $\mathcal{P}_{\text{def}}^{*}$				
	$\mathcal{P}$		$\mathcal{P}^{*}$	
	ϵ	Incr.	ϵ	Incr.
Default	0.24	+0%	0.12	+0%
$h = 0.5$ m	0.29	+21%	0.16	+33%
$h = 2.0$ m	0.22	-9%	0.11	-9%
$E = 2.5$ GPa	0.25	+4%	0.14	+17%
$E = 10$ GPa	0.24	+0%	0.13	+8%
$\sigma_{\text{fl}} = 250$ kPa	0.25	+4%	0.22	+83%
$\sigma_{\text{fl}} = 1$ MPa	0.25	+4%	0.16	+33%
$\sigma_{\text{cr}} = 300$ kPa	0.22	-9%	0.12	+0%
$\sigma_{\text{cr}} = 1.2$ MPa	0.29	+21%	0.21	+75%
$H = 50$ m	0.24	+0%	0.12	+0%
$H = 200$ m	0.25	+4%	0.12	+0%
$\theta = 30°$	0.29	+21%	0.17	+42%
$\theta = 60°$	0.25	+4%	0.13	+8%

Table 1. The increase in the error ε when using $\mathcal{M}_{\text{eHD}}\left(\mathcal{P}_{\text{def}}\right)$ and $\mathcal{M}_{\text{eHD}}\left(\mathcal{P}_{\text{def}}^{*}\right)$ independently of changes in the physical parameters of the system. The column with the header `$\varepsilon$' lists the error for the listed change in the parameter. The column with header `Incr.' lists the increase

in error relative to the error for the default set of parameters which is 0.24 and 0.12, respectively.

Table 1 shows that the performance of $\mathcal{M}_{\text{eHD}}\left(\mathcal{P}_{\text{def}}\right)$ is insensitive to change in Young's modulus E, flexural strength σ_{fl}, and water depth H. Changes in the ice thickness h, crushing strength σ_{cr} and hull angle θ result in a medium increase in error. Overall it can be concluded that $\mathcal{M}_{\text{eHD}}\left(\mathcal{P}_{\text{def}}\right)$ is fairly insensitive to changes in the parameter set and is, therefore, quite robust.

The performance of $\mathcal{M}_{\text{eHD}}\left(\mathcal{P}^{*}_{\text{def}}\right)$ is also insensitive to changes in the water depth H, mildly sensitive to changes in ice thickness h, Young's modulus E, hull angle θ, and very sensitive to changes in flexural strength σ_{fl}, crushing strength σ_{cr}. It is also important to note that despite the larger relative increase in error, the error of $\mathcal{M}_{\text{eHD}}\left(\mathcal{P}^{*}_{\text{def}}\right)$ is smaller than the error of $\mathcal{M}_{\text{eHD}}\left(\mathcal{P}_{\text{def}}\right)$ for all cases considered.

In order to visualize what the increase in error mean in terms of deterioration of the prediction of both models, their predictions for one the worst cases, namely when σ_{fl} is set to 250 kPa, are shown in Fig. 5. Despite this increase in error, both models still perform better than $\mathcal{M}_{\text{HS}}$.

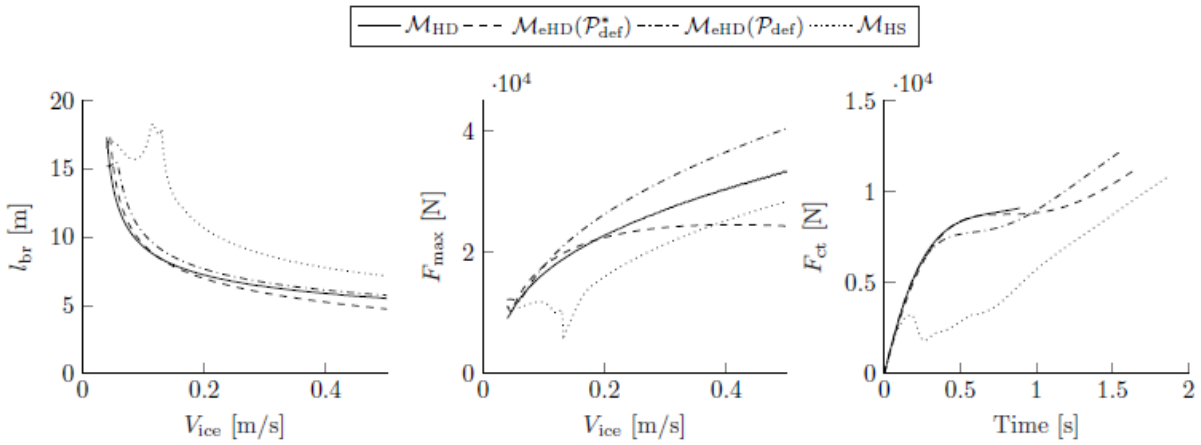

Figure 5. The performance of $\mathcal{M}_{\text{eHD}}\left(\mathcal{P}_{\text{def}}\right)$ and $\mathcal{M}_{\text{eHD}}\left(\mathcal{P}^{*}_{\text{def}}\right)$ when σ_{fl} is changed to 250 kPa. For the right graph $V_{\text{ice}} = 0.04$ m/s.

Even though $\mathcal{M}_{\text{eHD}}$ is a fairly robust model as shown by Table 1, there might be situations in which changing the parameters is desirable in order to minimize the error. As such, the optimization process was redone for each change in parameter, resulting in the sets of coefficients listed in Table 2. The table shows that when the optimization is redone when the physical parameters are changed, the error of both $\mathcal{M}_{\text{eHD}}\left(\mathcal{P}_{\text{def}}\right)$ and $\mathcal{M}_{\text{eHD}}\left(\mathcal{P}^{*}_{\text{def}}\right)$ remains of the same order of magnitude.

Optimal sets of coefficients							
	$\mathcal{P}$			$\mathcal{P}^*$			
	C_m [-]	ξ_d [-]	ϵ [-]	C_m [-]	ξ_d [-]	C_bc 10^{-6} [m^2]	ϵ [-]
Default	2.83	1.46	0.24	6.26	1.06	4.85	0.12
$h = 0.5$ m	2.73	2.19	0.27	6.16	1.56	4.36	0.15
$h = 2.0$ m	2.83	0.96	0.21	6.16	0.56	4.36	0.09
$E = 2.5$ GPa	3.03	1.33	0.25	6.46	0.92	6.18	0.12
$E = 10$ GPa	2.73	1.60	0.24	6.16	1.19	4.00	0.11
$\sigma_\mathrm{fl} = 250$ kPa	2.83	1.65	0.24	3.84	1.51	2.06	0.11
$\sigma_\mathrm{fl} = 1$ MPa	4.55	1.10	0.24	9.19	0.69	9.82	0.10
$\sigma_\mathrm{cr} = 300$ kPa	3.03	1.06	0.21	6.57	0.69	6.55	0.09
$\sigma_\mathrm{cr} = 1.2$ Mpa	2.53	2.10	0.28	6.26	1.37	3.64	0.15
$H = 50$ m	2.83	1.46	0.24	6.16	1.06	4.73	0.12
$H = 200$ m	2.73	1.46	0.25	6.26	1.10	5.09	0.12
$\theta = 30°$	3.33	1.87	0.27	8.69	0.01	7.27	0.14
$\theta = 60°$	2.42	1.01	0.23	6.26	0.78	3.88	0.10

Table 2. The sets of optimal coefficients for a range of system parameters and the resulting error.

DISCUSSION

Comparison with other effective fluid models

Two other studies have investigated using an EFM in the context of the hydrodynamic response of elastic ice as mentioned in the introduction. It is interesting to compare those models with the EFM proposed in this paper.

First, the possibility of using a frequency-independent added mass coefficient for the dynamical uplift of level ice was investigated by Dempsey and Zhao (Zhao & Dempsey 1992; Dempsey & Zhao 1993; Zhao & Dempsey 1996). All three studies concluded that this approach cannot reproduce the effects of hydrodynamics because the wave motion is fundamentally different when hydrodynamics is included. Although these studies do not consider ice-slope interaction, it is interesting to assess how the proposed EFM performs when only an added mass coefficient is used, i.e. when $\xi_\mathrm{d} = C_\mathrm{bc} = 0$. The optimal value of c_m for the default set of parameters is 4.44 [-]. In the papers by Dempsey and Zhao papers, the main prediction that was studied was $F_\mathrm{ct}(t)$. Fig. 6 shows that $F_\mathrm{ct}(t)$ is also poorly predicted by the proposed EFM when $\xi_\mathrm{d} = C_\mathrm{bc} = 0$. From this, it can be concluded that added damping is an essential component of the EFM, a finding that is supported by the observations regarding the effects of hydrodynamics on ice-slope interaction.

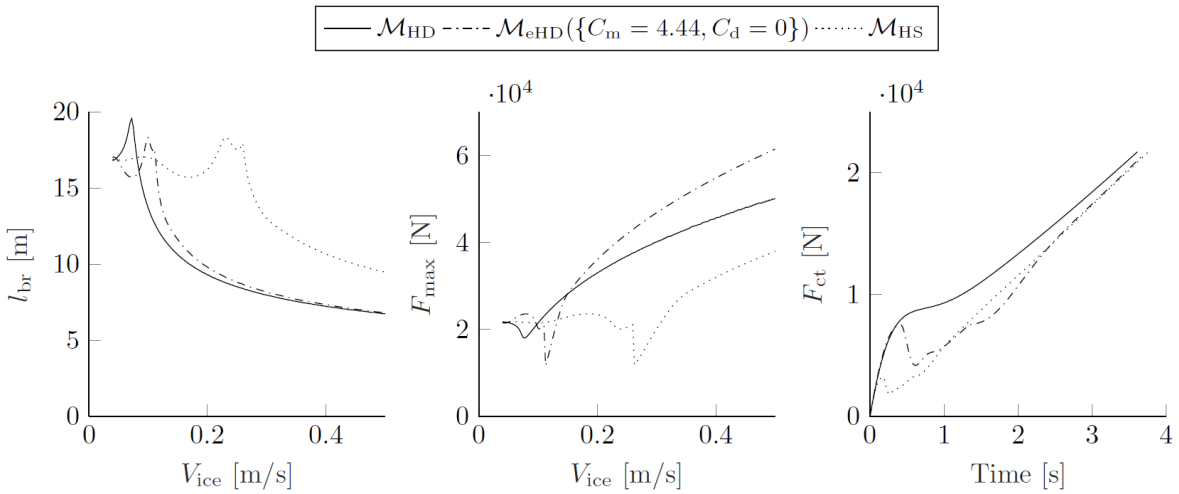

Figure 6. The performance of $\mathcal{M}_{\mathrm{eHD}}\left(C_m = 4.44, \xi_{\mathrm{d}} = C_{\mathrm{bc}} = 0\right)$ for the default set of parameters. For the right graph $V_{\mathrm{ice}} = 0.04$ m/s.

Secondly, (Lubbad et al. 2008) studied using a frequency-independent added mass and damping coefficient for ice-slope interaction. However, the difference with the proposed EFM is that the added damping term was multiplied with the squared fluid velocity. They found that this damping term had a marginal influence on the response of the ice. Therefore, this model also only considered added mass and it is, therefore, likely that this is the reasons for the unsatisfactory agreement with their hydrodynamic reference model.

Applicability of the proposed effective fluid models

Although the proposed effective fluid models greatly improve the predictions of $\mathcal{M}_{\mathrm{HS}}$, several reservations are in order. Firstly, in this study, only the interaction with a sloping structure was considered. The applicability of the EFM to other cases, like the uplift scenarios considered in (Dempsey & Zhao 1993; Zhao & Dempsey 1996) or interaction between individual ice floes, has yet to be investigated. Moreover, as the current model is 2D, its applicability for ice-slope interaction in 3D is unknown.

CONCLUSIONS

In this paper, an effective fluid model was presented that can accurately reproduce the effects that hydrodynamics has on ice-slope interaction. This fluid model can be added to existing ice-sloping interaction model that only includes hydrostatics with minimal effort. The resulting effective ice-slope interaction model is very simple but its predictions are significantly better than a hydrostatic model. The model is also fairly robust in that its predictions remain accurate even when the physical parameters of the system are changed. While the applicability of the proposed fluid model to a wider range of IFI problems remains to be investigated, the proposed approach is very promising.

REFERENCES

Dempsey, J.P. & Zhao, Z.G., 1993. Elastohydrodynamic response of an ice sheet to forced sub-surface uplift. *Journal of the Mechanics and Physics of Solids*, 41(3), pp.487–506.

Engelund, F., 1966. *Added Moment of Inertia for a Rotating Plate*, Coastal Engineering Laboratory, Hydraulic Laboratory, Technical University of Denmark.

Jensen, F.B. et al., 2011. *Computational Ocean Acoustics*, New York, NY: Springer New York. Available at: http://link.springer.com/10.1007/978-1-4419-8678-8.

Keijdener, C., Hendrikse, H. & Metrikine, A., 2018. The effect of hydrodynamics on the bending failure of level ice. *Cold Regions Science and Technology*, 153(May), pp.106–119.

Keijdener, C. & Metrikine, A., 2014. The effect of ice velocity on the breaking length of level ice failing in downward bending. *Proceedings of 22nd IAHR International Symposium on Ice*.

Lubbad, R., Moe, G. & Løset, S., 2008. Static and dynamic interaction of floating wedgeshaped ice beams and sloping structures. In *Proceedings of the 19th IAHR Symposium on Ice, Vancouver, Canada*. pp. 227–237.

Sawamura, J., Riska, K. & Moan, T., 2008. Finite element analysis of fluid-ice interaction during ice bending. In *Proceedings of the 19th IAHR Symposium on Ice, Vancouver, Canada*. pp. 239–250.

Sørensen, C., 1978. Dynamic response of a semi-infinite plate subjected to steadily increasing boundary force. *ZAMM 58*, p.T 126-T 128.

Stoker, J.J., 1992. *Water Waves*, Hoboken, NJ, USA: John Wiley & Sons, Inc. Available at: http://doi.wiley.com/10.1002/9781118033159.

Valanto, P., 2006. On the Ice Load Distribution on Ship Hulls in Level Ice. *Icetech 2006*, pp.1–10.

Valanto, P., 1992. The icebreaking problem in two dimensions : experiments and theory. *Journal of Ship Research*, 36(4), pp.299–316.

Valanto, P., 2001. The resistance of ship in level ice. *Transactions of the Society of Naval Architects and Marine Engineers*, 109, pp.53–83.

Wang, Y. & Poh, L.H., 2017. Velocity effect on the bending failure of ice sheets against wide sloping structures. *Journal of Offshore Mechanics and Arctic Engineering*, 139(6), p.061501. Available at: http://offshoremechanics.asmedigitalcollection.asme.org/article.aspx?doi=10.1115/1.4036478.

Williams, T.D. & Squire, V.A., 2008. The effect of submergence on wave scattering across a transition between two floating flexible plates. *Wave Motion*, 45(3), pp.361–379.

Zhao, Z.G. & Dempsey, J., 1992. A dynamically forced floating beam. In *IAHR Ice Symposium*. Banff, Alberta.

Zhao, Z.G. & Dempsey, J.P., 1996. Planar forcing of floating ice sheets. *International Journal of Solids and Structures*, 33(1), pp.19–31.